NUMERICAL ANALYSIS OF SHRINKAGE STRESSES IN A MASS CONCRETE

How-Ji Chen*, Hsien-Sheng Peng, and Yi-Feng Chen

ABSTRACT

A numerical model based on an actual structure in Taiwan is proposed to investigate the shrinkage behavior of mass concrete. A commercially available program, ANSYS, which treats concrete as a homogeneous and isotropic material, was used in the investigation. The stresses are assumed to be within the elastic range. The shrinkage strains for various segments of mass concrete were evaluated according to currently available prediction equations (ACI 209, 1992; CEB-FIP, 1991). By converting these strain values into equivalent stresses based on Hook's law, finite element computations were then performed to predict the long-term shrinkage behavior of mass concrete.

Experimental verifications by nondestructive tests were carried out to confirm the results of the numerical predictions. Comparisons show that the numerical predictions are in agreement with the experimental results.

Key Words: mass concrete, shrinkage stresses, finite element, nondestructive test.

I. INTRODUCTION

After being used for a long time, cracks in mass concrete may be found on the surface of a structure. This is due to a change of volume caused by the drying shrinkage of concrete (Mehta, 1986). The drying shrinkage of mass concrete is mainly caused by the uneven distribution of humidity, which also leads to different shrinkage strains in different sections (Mindess and Young, 1981; Kim and Lee, 1998). Accurate evaluation of the amount of concrete shrinkage is very important for pre-stressed concrete design and predicting cracking in mass concrete. Investigators have proposed equations to predict the drying shrinkage strain of concrete (ACI 209, 1992; CEB-FIP, 1991). However, these equations do not yield the same results. Hence, engineers and researchers have tried to learn how to predict the drying shrinkage strain in mass concrete precisely, as well as the effect of drying shrinkage upon mass concrete.

A concrete cylindrical container (10.4 m in diameter, 10.8 m in height and 2.5 m thick, built on a 3 m thick foundation plate), located at the Institute of Nuclear Energy Research in Taiwan, was selected as the prototype structure for measurements and analyses of actual cracks and shrinkage. The numerical model is established based on the real scale of the mass concrete structure to permit analysis by the ANSYS program. The drying shrinkage strain in different sections of mass concrete structures was evaluated in accordance with various prediction equations. The calculated drying shrinkage strain is then transformed into equivalent stress according to the general Hook's law, which is then applied to the mass concrete model. Strains corresponding to equivalent stress were used to simulate the drying shrinkage strain. Finally, a nondestructive test, base on the Time-of-Flight Diffraction Technique (Lin and Su, 1996; Lin *et al.*, 1999), is carried out to measure the depth of cracks and to confirm the results of the numerical predictions.

II. CONCEPT OF EQUIVALENT STRESS

Since the value of concrete strain cannot be considered as an input, the drying shrinkage strain is transformed into an equivalent stress in numerical calculations. It is assumed that the materials are homogeneous and elastic; the relationship between the

*Corresponding author. (Tel: 886-4-22859390; Fax: 886-4-22855610; ; Email: hjchen@mail.ce.nchu.edu.tw)

The authors are with the Department of Civil Engineering, National Chung-Hsing University, Taichung, Taiwan 402, R.O.C.

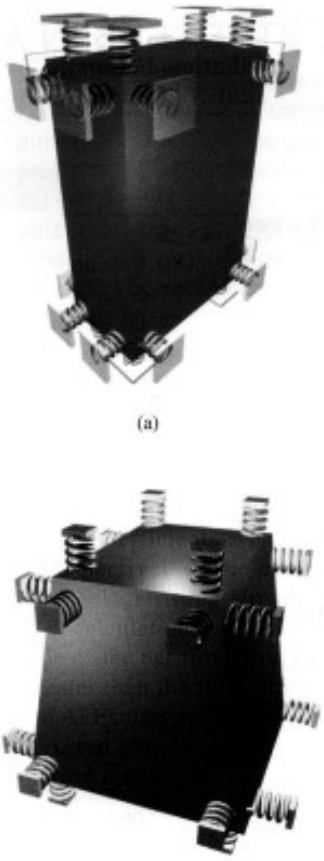

Fig. 1 3-D solid element

drying shrinkage strain and the equivalent stress can be derived according to the general Hook's law.

The stress-strain formula of the general Hook's law is

$$\varepsilon_x + \varepsilon_y + \varepsilon_z = \frac{1-2\nu}{E}(\sigma_x + \sigma_y + \sigma_z) \quad (1)$$

where ν is Poisson's ratio, E is elastic modulus, ε and σ represent respectively the strain and stress; the subscripts denote the directions of the Cartesian axes.

Suppose that the element would shrink homogeneously, so the strains and stresses on the three axes are isotropic. Therefore, one has

$$\Rightarrow \sigma = \frac{E}{1-2\nu}\varepsilon \quad (2)$$

where ε and σ represent respectively the drying shrinkage strain and equivalent stress.

Two different shape elements and a beam model were chosen for verifying the applicability of the concept of equivalent stress. By using an element (Solid Brick 8 nodes 45 element) with a 2:1:3 aspect ratio (length, width and height), a linear spring (Beam 4 element) is added at each node in three directions with stiffness approaching zero (see Fig. 1(a)). The material parameters were used according to the actual concrete data, which are E=21.3 GPa, ν=0.2, and the drying shrinkage strain was assumed 500 μ. The equivalent stress calculated by the conversion formula (2) is 17.75 MPa. Tri-axial uniform stress was placed onto the element for calculation. The results of drying shrinkage strains in the X, Y, and Z-axis directions are all 500 μ, the same as the assumed value. Another analysis performed used a tapered element as shown in Fig. 1(b). All parameters used are the same as for the element described above. After calculation, the drying shrinkage strains in X, Y, and Z-axis directions can be determined to be 500 μ, respectively. The strain result of the finite element analysis shows that the concept of equivalent stress is feasible. However, the corresponding stress result is not the real stress caused by shrinkage. The original equivalent stress must be subtracted from the result after analysis. In order to verify the point, a beam frame (the numerical model as shown in Fig. 2) is analyzed. Suppose that each element of this beam endures 800 μ shrinkage strain in the Z-axis direction. The comparison of theoretical and numerical solutions at three different places on this beam is listed in Table 1. Due to the boundary condition of the two fixed ends, the numerical solution of strain in the Z-axis direction approaches zero. We find that the

Table 1 Comparison of theoretical and numerical solutions

	Beam	$L/4$	$L/2$	$3L/4$
σ_z (MPa)	Numerical solution	17.06	17.06	17.06
	Theoretical solution	17.06	17.06	17.06
ε_z	Numerical solution	1.17E-18	-1.17E-19	-1.17E-18
	Theoretical solution	0	0	0

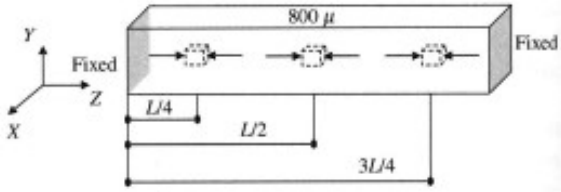

Fig. 2 Beam model

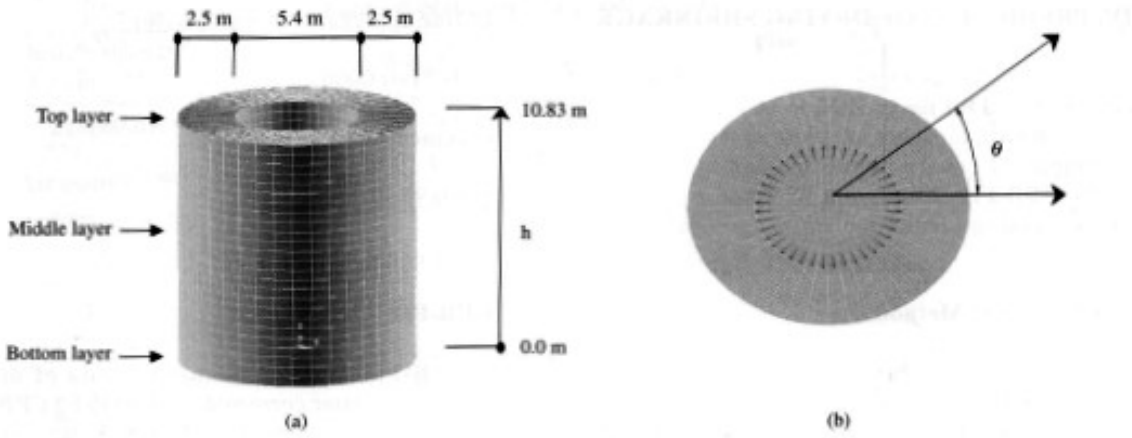

Fig. 3 Numerical model of mass concrete

theoretical solution is also zero. As to stress, after subtracting equivalent stress from the numerical solution, the solution is as same as the theoretical one (shown in Table 1). The result verified the applicability of the concept of equivalent stress.

Shrinkage is not the same in every part of a mass concrete structure. Three prediction formulas, the specification of ACI 209 (1992), CEB-FIP (1991) and the formula proposed by Kim and Lee (1998), were used to determine the amount of drying shrinkage strain. Stress and strain caused by shrinkage can be obtained according to the equivalent stress concept.

III. RELIABILITY OF NUMERICAL CALCULATION

The precision of numerical calculation depends on whether the result is convergent after calculation. Different mesh methods were used to test the precision of the numerical calculation. A uniform distributed stress P applied from inside radiates toward the outside to simulate a container enduring an internal exploding stress. The numerical model is of a container with a circular wall and solid plate bottom (as shown in Fig. 3). The aspect ratio of element is kept under 4 and the inside angle at each corner is between 45° and 135°. An internal pressure of 50 MPa is applied. Considering the actual boundary condition of the container, the center of the bottom is fixed in three directions (X, Y, and Z-axis) and the other parts of the bottom are only constrained in the Z direction, the circular wall is free. The material parameter is compressive strength (fc')=20 MPa, E=21.3 GPa and ν=0.2. The result of the numerical calculation (Fig. 4) shows that if more than 10,000 elements are used, both principal stress and strain converge. If it is greater than 15,000, no matter what meshing

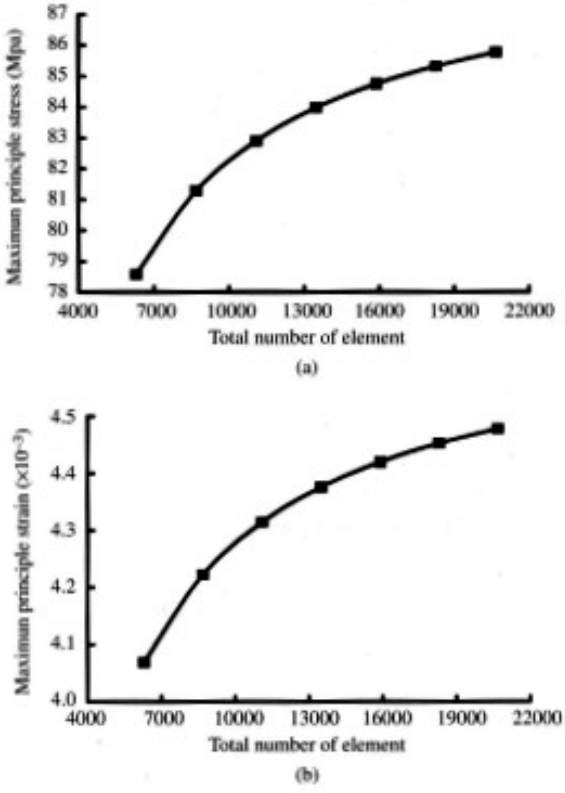

Fig. 4 Maximum principal stresses and strains of mass concrete

methods we choose, the result is almost the same. The maximum deviation of the principal stress or principal strain is within ±0.5%. That means the proposed mesh method is very precise. Therefore, a total element number over 15,000 is adopted for the following analysis.

IV. PREDICTION OF DRYING SHRINKAGE

There are many empirical equations that have been developed for the prediction of shrinkage. The most common approaches are those of ACI and CEB. The empirical equations recommend by ACI 209 (1992), CEB-FIP (1991) and Kim and Lee (1998) were adopted to predict the shrinkage strain inside mass concrete.

1. ACI 209R-92 Method

ACI Committee 209 recommended this empirical equation in 1992 that allows shrinkage to be estimated as a function of time of drying and ultimate shrinkage. The shrinkage, $(\varepsilon_{sh})_t$, at any time t after age 7 days for moist cured concrete is given by

$$(\varepsilon_{sh})_t = \frac{t}{35+t}(\varepsilon_{sh})_u \tag{3}$$

where $(\varepsilon_{sh})_u$ is the value of ultimate shrinkage. The effect of others properties of concrete are given by correction factors:

$$(\varepsilon_{sh})_u = 780\gamma_{cp}\cdot\gamma_\lambda\cdot\gamma_h(\gamma_{vs})\cdot\gamma_s\cdot\gamma_\varphi\gamma_\alpha\times10^{-6} \tag{4}$$

where

1. $\gamma_{cp} = \begin{cases} 1.2, & t_1 = 1 \\ 1.1, & t_1 = 3 \\ 1.0, & t_1 = 7 \\ 0.93, & t_1 = 14 \\ 0.86, & t_1 = 28 \\ 0.75, & t_1 = 90 \end{cases}$

   t_1: initial moist curing days

2. $\gamma_\lambda = \begin{cases} 1.40 - 0.010\lambda, & \text{for } 40 \le \lambda \le 80 \\ 3.00 - 0.030\lambda, & \text{for } 80 < \lambda \le 100 \end{cases}$

   λ: relative humidity (%)

3. $\gamma_{vs}=1.2\exp(-0.00472\ v/s)$

   v/s: volume to surface ratio

4. $\gamma_s=0.89+0.00161s$

   s: slump (mm)

5. $\gamma_\varphi = \begin{cases} 0.3 + 0.0024\varphi, & \text{for } \varphi \le 50\% \\ 0.90 + 0.002\varphi, & \text{for } \varphi > 50\% \end{cases}$

   φ: fine aggregate percentage (%)

6. $\gamma_c=0.75+0.00061c$

   c: cement content (kg)

7. $\gamma_\alpha= 0.95+0.008\alpha$

   α: air content (%)

2. CEB-FIP 1990 Method

CEB-FIP 1978 prediction formula of drying shrinkage was later corrected in 1990 to be CEB-FIP 1990. The traditional CEB-FIP 1978 tends to neglect some material parameters; hence, its predictions are relatively weak. The corrected CEB-FIP 1990, however, considers the material parameters of 28-day compressive strength and types of cement. The detailed prediction formula is as follows:

$$\varepsilon_{cs}=\varepsilon_{cso}\cdot\beta_s(t-t_s) \tag{5}$$

where ε_{cs} is the shrinkage strain at time t after drying commences at time t_s; ε_{cso} is the basic shrinkage coefficient, which depends on relative humidity, type of cement and compressive strength of concrete. ε_{cso} is given by

$$\varepsilon_{cso}=\varepsilon_s(f_{cm})\cdot\beta_{RH} \tag{6}$$

where

$$\varepsilon_s(f_{cm}) = [160+10\beta_{sc}(9-\frac{f_{cm}}{f_{cmo}})]10^{-6}$$

f_{cm} = compressive strength (MPa)
f_{cmo} = 10 MPa
β_{sc} = 4, low heat cement
5, normal cement
8, high early strength cement

$$\beta_{RH} = \begin{cases} -1.55\cdot\beta_{sRH}, & 40\% \le RH \le 99\% \\ +0.25, & RH \ge 99\% \end{cases}$$

$$\beta_{sRH} = 1-(\frac{RH}{RH_0})^3$$

RH = relative humidity (%)
RH_0 = 100%

β_s is a function corresponding to the change of shrinkage with time, which depends on specimen dimensions, is given by

$$\beta_s(t-t_s) = [\frac{(t-t_s)/t_1}{350(h/h_0)^2+(t-t_s)/t_1}]^{0.5} \tag{7}$$

where

Table 2 Data used in prediction formulas

Design strength (kg/cm^2)(MPa)	Slump (mm)	Water (kg/m^3)	Cement (kg/m^3)	Fine aggregate (kg/m^3)	Coarse aggregate (kg/m^3)
210(20.6)	100	185	280	799	1056
Air content (%)	R. H. (%)	Curing time (days)	Type of cement	Prediction strength (kg/cm^2)(MPa)	
2	70	14	Type I Portland cement	280(27.5)	

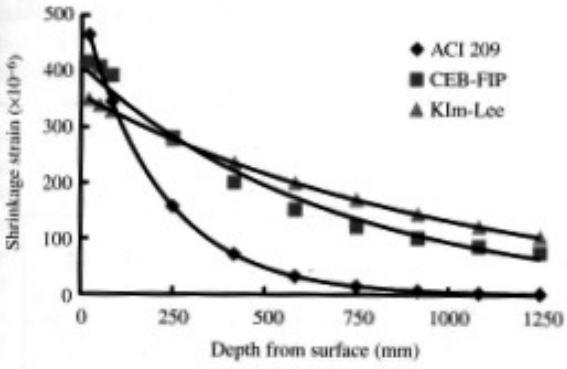

Fig. 5 Prediction of concrete shrinkage strain at 20 years of age

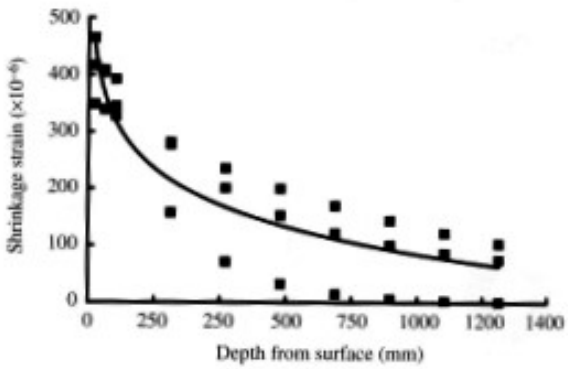

Fig. 6 Averaged shrinkage strain

h = $2A_c/u$ (mm)
A_c = cross section (mm^2)
u = perimeter (mm)
t_1 = 1 day
h_0 = 100mm

3. Kim and Lee Method

The prediction equation proposed by Kim and Lee (1998) allows shrinkage to be estimated as a function of time of drying and length of the diffusion path. The shrinkage, $\varepsilon(y, t)$, is given by

$$\varepsilon(y, t)=ae^{b\lambda} \tag{8}$$

where

a : 353×10^{-6} for w/c 0.65
238×10^{-6} for w/c 0.40
b : -415.4 for w/c 0.65
-426.1 for w/c 0.40
λ : $y/\sqrt{t}$
y : length of the diffusion path (m)
t : shrinkage hours

All data needed in the prediction formula (Table 2) are based on the design information of the con-tainer. For comparisons, the predictions are carried out up to 20 years, which are the current service period of the container. The results of the predictions are shown in Fig. 5. It can be seen that the predictions of the shrinkage strains according to the CEB and Kim-Lee formulas are very close. The result according to the ACI prediction formula, however, is significantly different. To obtain a neutral prediction, the results of the three prediction formulas are averaged out and the average drying shrinkage strain is shown in Fig. 6. From the results of Figs. 5 and 6, we can get the drying shrinkage strain on any section in the container. The top surface (in vertical direction) of the container (see Fig. 3) was covered by mortar of over 100 mm. The bottom surface (in vertical direction) was built on a continuous foundation plate (3 m thick). Therefore, both surfaces are considered as closed surfaces and the water diffusion path in this direction is ignored. The value is then transformed to equivalent stress for numerical calculation. The respective equivalent stress is shown in Table 3 while the corresponding element position and serial numbers are shown in Fig. 7.

V. NUMERICAL ANALYSIS

The drying shrinkage strains, averaged from

Table 3 Equivalent stresses at each element

Serial number of element		8	7, 9	6, 10	5, 11	4, 12	3, 13	2, 14	1, 15
Averaged (ACI – 209, CEB – FIP, Kim – Lee)	Shrinkage strain ($\times 10^{-6}$)	63	77	93	111	135	167	215	319
	Equivalent stress (MPa)	2.25	2.73	3.29	3.96	4.8	5.93	7.64	11.33
ACI-209	Shrinkage strain ($\times 10^{-6}$)	1	3	7	15	33	72	157	345
	Equivalent stress (MPa)	0.05	0.11	0.24	0.53	1.16	2.54	5.58	12.26
CEB-FIP	Shrinkage strain ($\times 10^{-6}$)	75	86	101	122	152	201	282	392
	Equivalent stress (MPa)	2.66	3.06	3.58	4.32	5.41	7.13	10.01	13.94

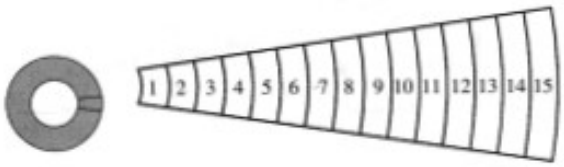

Fig. 7 Arrangement of elements

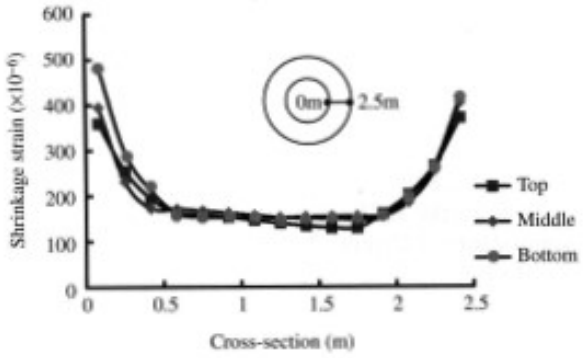

Fig. 8 Radial distributions of shrinkage strains at different heights

the results of the three prediction formulas (see Fig. 6), were used to predict the drying shrinkage behavior of the container. The results of the numerical calculation from the top layer, the middle layer and the bottom layer of the numerical model of container (see Fig. 3) are shown in Figs. 8 and 9.

The maximum principal strains caused by drying shrinkage of concrete are shown in Fig. 8. The figure shows that mass concrete will shrink after long-term drying shrinkage. In the interior of concrete, the drying shrinkage strain gradient is relatively mild and the principal strains are smaller at about -150 μ.

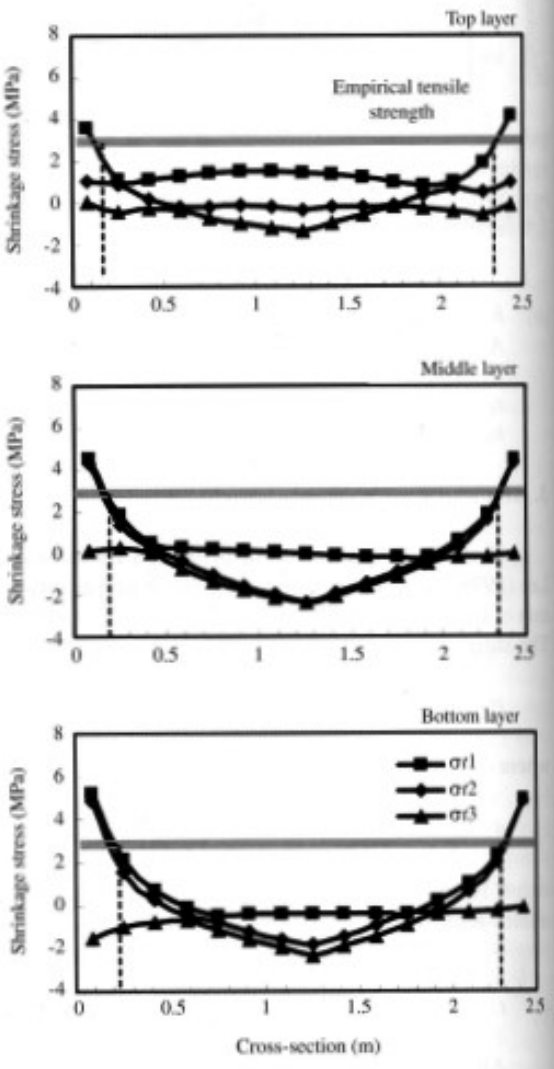

Fig. 9 Radial distributions of principal stresses (averaged model)

Larger strains appeared in the area near the surface. The maximum strain value, -485 μ, is found on the bottom layer of the mass concrete surface. The main reason for this is the interaction between the drying shrinkage of the concrete body and the constraint of the concrete bottom. The result is in accordance with the theoretical prediction.

Fig. 9 shows the result of the principal stress of concrete caused by drying shrinkage strain. The principal stress lies between -2.41 MPa and 5.22 MPa. The stresses distributed on the interior sections of concrete are compressive stresses. The ones on the sections near surface are tensile stresses. The maximum tensile stress is found in the surface area of the bottom, as it is influenced by the constraint of the boundary condition.

Tensile strength is an important property of concrete that greatly affects the extent and the size of cracking in structures. Most literature (Mehta, 1986; Mindess and Young, 1981) holds that the tensile/compressive strength ratio depends on the level of compressive strength, the higher the compressive strength, the lower the ratio. In general, the ratio of tensile strength to compressive strength ranges from 0.07 to 0.14. In this study, a more conservative value of 10 to 12.5% compressive strength is used to predict stress that may cause cracking on the concrete. Fig. 9 shows that the tensile stresses distribute on the top layer near the surface area exceed the predicted value of cracking stress. The tensile stress of the remaining area will not lead to the occurrence of cracks. From the figure, we can determine that the depth of cracks at the top layer of the mass concrete is about 0.2 m. The principal stress results at the middle layer of the container (Fig. 9) show that the surface area of the concrete is under tensile conditions and the interior of the concrete is under compressive conditions. The depth of the cracks is also determined to be about 0.2 m. The principal stress at the bottom layer of the container is similar to the distribution at the middle layer, but the tensile stress of the surface area is little higher than those of the middle layer or the top layer. The reason is that it is influenced by the boundary conditions. The possible crack depth is also the same as middle layer at 0.2 m.

The drying shrinkage behavior of the container, predicted based on the shrinkage strains calculated from the ACI 209 formula and the CEB-FIP formula (see Fig. 5), are shown in Figs. 10 and 11. The results show that the distribution of principal stress is similar to the above-mentioned result. The only difference is that the predicted depths of cracks of the ACI mode are shallower. The top layer is about 0.2 m, the middle layer is about 0.2 m and the bottom layer is about 0.2 m. On the other hand, the predicted depths of CEB-FIP mode are deeper. The top layer

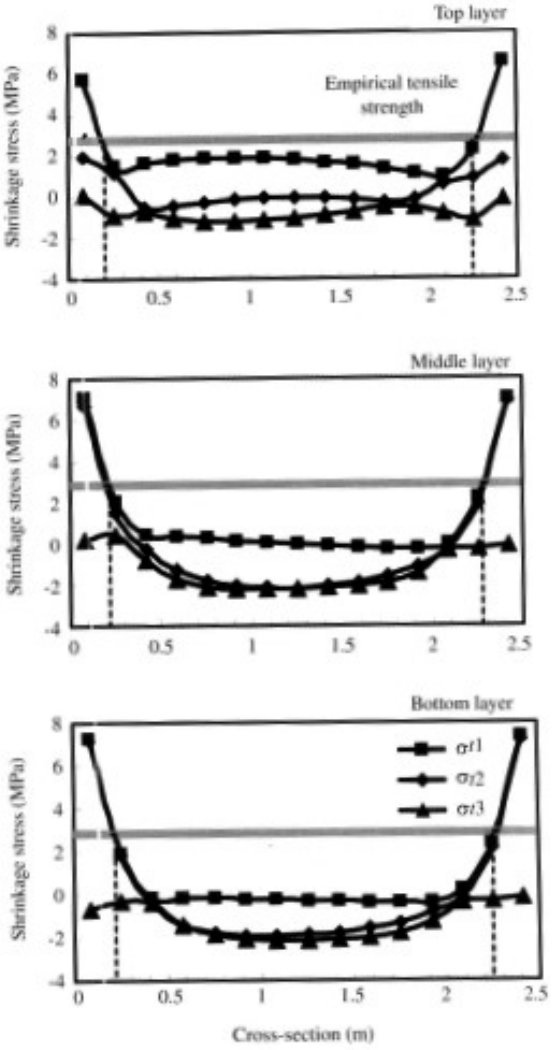

Fig. 10 Racial distributions of principal stresses (ACI 209 model)

is about 0.2 m, the middle layer is about 0.2 m and the bottom layer is about 0.2 m. The predicted drying shrinkage strain of the ACI 209 formula has a greater gradient near the surface area, but the affected depth is shallower. The tensile stress at the surface area is larger, which leads to a shallower crack depth. The results of the CEB-FIP mode show a smaller tensile stress at the surface area and deeper cracks. This is because its shrinkage gradient is milder than that of ACI 209. Therefore, although the concrete surface appears to have lower tensile stress, the affected depth is deeper and a deeper crack will be predicted (see Figs. 10 and 11). In summary, the stress distribution predicted by the ACI 209 and CEB-FIP formulas is similar to the result of analysis from the average of the three prediction formulas (see Fig. 9).

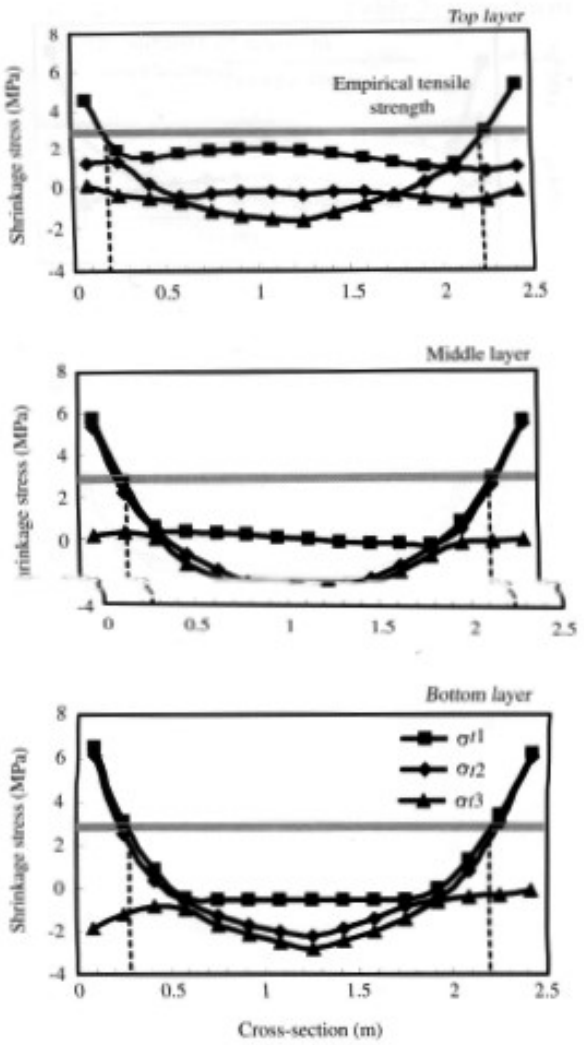

Fig. 11 Radial distributions of principal stresses (CEB-FIP model)

Meanwhile, the predicted depths of the cracks are close.

VI. NONDESTRUCTIVE TEST

A nondestructive test (Impact Echo) was chosen for determining the crack depths in the concrete. The test is economical, rapid and does not cause any damage in the concrete. The cracks of the container measured by nondestructive test are shown in Table 4. The corresponding positions of the cracks are shown in Fig. 3. The result shows that the cracks on the container mostly concentrate on the surface area at an altitude of 4~7 m and crack depth varies from 0.07–0.14 m. The numerically predicted crack depth is about 0.2 m. The two results are not the same.

Table 4 Nondestructive test results

Number	Crack widths (mm)	Location (θ, h)	Crack depths (mm)
1	0.2	(3°, 6.5 m)	75
2	0.2	(90°, 7.0 m)	130
3	0.2	(15°, 7.5 m)	120
4	0.2	(18°, 6.0 m)	133
5	0.1	(31°, 6.5 m)	120
6	0.1	(115°, 5.5 m)	125
7	0.1	(128°, 6.5 m)	115
8	0.2	(340°, 4.5 m)	114
9	0.2	(350°, 4.5 m)	137

This situation might be caused by not considering the reinforcing bars in the analysis model. The depth of top reinforcing bar in the whole building is 75 mm. The reinforcing bar can share part of the tensile stress and reduce the occurrence of drying shrinkage cracks. Although the reinforcing bar is not considered and the result cannot reflect a real situation, the predicted depth of cracks is reliable for the concrete cover region of the container. Comparison of the numerical prediction result and the nondestructive test data shows that the two results are close and acceptable. This verifies that the proposed method is reliable.

VII. CONCLUSIONS

Numerical method is used to simulate the behavior of drying shrinkage and to predict crack depths in mass concrete. From the comparison of the numerical results and the nondestructive test results, the conclusions can be summarized as follow:

1. The numerical calculation result shows that a better convergence can be achieved if the aspect ratio (length, width and height) of the element is within 4 and the mesh angle of the element is between 45° and 135°. The maximum deviation of principal stress or principal strain is within ±0.5%.
2. Based on the general Hook's law, the calculated shrinkage strains in different sections of mass concrete are converted into equivalent stresses. The stresses are further applied in the numerical model to predict drying shrinkage behaviors. This approach is proven to be applicable.
3. The stress distribution situations of mass concrete predicted by the ACI 209 and CEB-FIP formulas are similar to the result gained by averaging the results of the three prediction formulas.
4. The ACI 209 prediction mode showed greater tensile stress near the surface area, but the affected depth is shallower and it predicted a shallower crack. The CEB-FIP prediction mode showed

smaller tensile stress at the surface area and deeper cracks.

5. As the prediction model does not consider the effect of reinforcing bars, the predicted crack depths are larger than those from the measurements.
6. Comparison of the numerical prediction result and the nondestructive test data shows that the numerical method to predict the shrinkage behavior of mass concrete is reliable.

ACKNOWLEDGMENTS

The authors would like to thank Professor Y. Lin for his experimental assistance during this project.

NOMENCLATURE

E	elastic modulus
fc'	compressive strength
β_s	a function corresponding to the change of shrinkage with time
ε	strain
$\varepsilon(y, t)$	the shrinkage estimated as a function of time of drying and length of the diffusion path
ε_{cs}	the shrinkage strain at time t after drying commences at time t_s
ε_{cso}	the basic shrinkage coefficient
$(\varepsilon_{sh})_t$	drying shrinkage at any time t after age 7 days for moist cured concrete
$(\varepsilon_{sh})_u$	the value of ultimate shrinkage
ν	Poisson's ratio
σ	stress

REFERENCES

ACI Committee 209, 1992, "Prediction of Creep, Shrinkage and Temperature Effects in Concrete Structure," *American Concrete Institute*, Farmington Hills, MI, USA.

CEB-FIP, 1991, "Model Code for Concrete 1990," *Final Draft, CEB Bulletin D'Information No. 203*, pp. 2.27-2.38, pp. 2.43-2.49.

Kim, J. K., and Lee, C. S., 1998, "Prediction of Differential Drying Shrinkage in Concrete," *Cement and Concrete Research*, Vol. 28, No. 7, pp. 985-994.

Lin, Y., Liou, T., and Tsai, W. H., 1999, "Determining the Crack Depth and the Measurement Errors Using Time-of-Flight Diffraction Techniques," *ACI Materials Journal*, Vol. 96, No. 2, pp. 190-195.

Lin, Y., and Su, W. C., 1996, "Use of Stress Waves for Determining the Depth of Surface-Opening Cracks in Concrete Structures," *ACI Materials Journal*, Vol. 93, No. 5, pp. 494-505.

Mehta, P. K., 1986, *Concrete: Structure, Properties, and Materials*, Prentice-Hall, Inc., Englewood Cliffs, NJ, USA.

Mindess, S., and Young, J. F., 1981, *Concrete*, Prentice-Hall, Inc., Englewood Cliffs, NJ, USA.

Manuscript Received: Sep. 25, 2002
Revision Received: Oct. 17, 2003
and Accepted: Nov. 21, 2003